

# Relevance of $4f$ - $3d$ exchange to finite-temperature magnetism of rare-earth permanent magnets: an *ab-initio*-based spin model approach for $\text{NdFe}_{12}\text{N}$

Munehisa Matsumoto<sup>1</sup>, Hisazumi Akai<sup>1,2</sup>, Yosuke Harashima<sup>1,3</sup>, Shotaro Doi<sup>1,2</sup>, Takashi Miyake<sup>1,3,1</sup>

<sup>1</sup>*Elements Strategy Initiative Center for Magnetic Materials (ESICMM), National Institute for Materials Science (NIMS), Sengen 1-2-1, Tsukuba 305-0047, JAPAN*

<sup>2</sup>*Institute for Solid State Physics, University of Tokyo, Kashiwa 277-8581, JAPAN,*

<sup>3</sup>*National Institute of Advanced Industrial Science and Technology (AIST), Umezono 1-1-1, Tsukuba 305-8568, JAPAN*

(Dated: 8 October 2018)

A classical spin model derived *ab initio* for rare-earth-based permanent magnet compounds is presented. Our target compound,  $\text{NdFe}_{12}\text{N}$ , is a material that goes beyond today's champion magnet compound  $\text{Nd}_2\text{Fe}_{14}\text{B}$  in its intrinsic magnetic properties with a simpler crystal structure. Calculated temperature dependence of the magnetization and the anisotropy field agree with the latest experimental results in the leading order. Having put the realistic observables under our numerical control, we propose that engineering  $5d$ -electron-mediated indirect exchange coupling between  $4f$ -electrons in Nd and  $3d$ -electrons from Fe would most critically help to enhance the material's utility over the operation-temperature range.

PACS numbers: 75.30.Gw, 75.50.Ww, 75.10.Hk, 75.10.Lp

## I. MOTIVATIONS

In the past three decades,  $\text{Nd}_2\text{Fe}_{14}\text{B}$ <sup>1</sup> has been the champion permanent magnet compound. A drawback of  $\text{Nd}_2\text{Fe}_{14}\text{B}$  has been its relatively low Curie temperature and that some practical applications require replacements of Nd with heavy-rare-earth (HRE) elements such as Dy and Tb to enhance the high-temperature coercivity, which is roughly proportional to the anisotropy field<sup>2</sup>. Since the HRE elements are less abundant, ways to achieve the equivalent magnetic properties to those of HRE-doped permanent magnets using only light rare-earth (LRE) elements have recently been sought after<sup>3</sup>. Also the relevance of understanding and controlling the finite-temperature magnetism of  $4f$ - $3d$  intermetallics is appreciated ever more.

A possible solution was recently suggested<sup>4</sup> by the material  $\text{NdFe}_{12}\text{N}$  stabilized in an almost bulk state<sup>5,6</sup>, where a newly fabricated film sample that consists of more than hundred unit-cell layers shows superior intrinsic magnetization and anisotropy field to  $\text{Nd}_2\text{Fe}_{14}\text{B}$ . The materials family,  $\text{RFe}_{12-x}\text{T}_x(\text{N})$  (R=rare earth), had actually been known for a long time<sup>7</sup> where the nitrogeneration pulls up the Curie temperature by 100-200 [K] and the magnetic anisotropy is enhanced as well, but the achieved magnetic properties were not on a par with the champion magnet compound  $\text{Nd}_2\text{Fe}_{14}\text{B}$  partially due to the necessity for the presence of the third element T=Ti etc. to stabilize the particular crystal structure. Recent breakthrough<sup>5</sup> made it possible to have  $\text{NdFe}_{12}$  without the third element in a sample fabricated as a thick film and nitriding achieved the intrinsic magnetic properties that goes beyond  $\text{Nd}_2\text{Fe}_{14}\text{B}$  at high temperatures<sup>5</sup>.

Thus we are motivated to theoretically address the finite-temperature magnetism of  $\text{NdFe}_{12}\text{N}$ . This would provide the prospect for its intrinsic magnetic properties, which serves to solve the high-temperature coer-

civity problem in LRE-based compounds. On the theory side, finite-temperature magnetism of rare-earth-based permanent-magnet materials poses a fundamentally challenging many-body problem: *ab initio* predictions mostly focus on the ground-state properties and the finite-temperature magnetism was discussed at best on the basis of a mean-field theory of a simplified model on the basis of a molecular field acting on an isolated rare-earth magnetic moment<sup>8-13</sup>. For comparison with experimentally observed magnetic anisotropy, contributions from  $3d$  electrons are sometimes added in an *ad hoc* manner. In principle, the theory of magnetism in  $4f$ - $3d$  intermetallics takes a description of the correlated electrons in  $4f$  and  $3d$ -orbitals, which may be done with a multi-orbital periodic Anderson model (PAM) with the conduction electrons composed of  $5d$ -band out of the rare-earth elements, harboring two species of impurities,  $3d$  and  $4f$ , each with the different levels of on-site electronic correlation.

In order to meet the urgent practical needs and also to provide a guideline data for future realistic simulations of PAM with huge number of orbitals, we exploit the essence of a simplified model<sup>14</sup> to describe only the low-energy effective physics of  $4f$ - $3d$  intermetallics with the model parameters determined as realistically as possible through *ab initio* calculations: we define a multi-sublattice spin model with one group of the sublattices describing the  $4f$ -originated localized magnetic moments and the other describing the  $3d$ -magnetization; the spins reside on a realistic lattice that mimicks the crystal structure of the given target material  $\text{NdFe}_{12}\text{N}$  with the *ab initio* input parameters. Note that the effective parameters, such as the strength of exchange couplings and crystalline electric fields, are determined as a consequence of the electronic states. They are target-material dependent, thus first-principles evaluation of the parameters is crucial for the quantitative modeling. Then we solve

the finite-temperature many-body problem with numerically exact Monte Carlo method to get the temperature dependence of magnetic observables and quantitatively compare with the latest experimental data. Our realistic lattice model is more realistic than were discussed in the previous works: The sublattice-specific character of each of the Nd and Fe atoms in the unit cell is taken into account on the basis of first principles, which is in contrast to a uniform molecular field imposed by Fe acting on rare-earth magnetic moments. Establishing the computational control of the intrinsic properties of magnetism of NdFe<sub>12</sub>N, we discuss within our model how to manipulate it to enhance its practical utility most effectively.

## II. THE REALISTIC-LATTICE SPIN MODEL

The spin model Hamiltonian defined on the lattice of the given crystal structure reads as follows.

$$\mathcal{H} = \mathcal{H}_T + \mathcal{H}_R + \mathcal{H}_{RT}, \quad (1)$$

$$\mathcal{H}_T = - \sum_{\langle i,j \rangle \in T} (2J_{ij}^{\text{TT}}) \mathbf{S}_i \cdot \mathbf{S}_j - \sum_{i \in T} D_i^{\text{T}} (S_i^z)^2, \quad (2)$$

$$\mathcal{H}_R = - \sum_{m \in R} D_m^{\text{R}} (J_m^z)^2, \quad (3)$$

$$\mathcal{H}_{RT} = \alpha_{\text{RT}} \sum_{\langle m,i \rangle, m \in R, i \in T} (2J_{mi}^{\text{RT}}) (g_J - 1) \mathbf{J}_m \cdot \mathbf{S}_i \quad (4)$$

We have denoted the lattice points on which  $3d$  ( $4f$ ) magnetic moments reside by  $T$  ( $R$ ), respectively. Here  $\mathbf{S}_i$  is a magnetic moment defined on site  $i$ ,  $J_{ij}$  is the exchange coupling between localized magnetic moments  $\mathbf{S}_i$  and  $\mathbf{S}_j$ , and  $D_i$  encodes the single-ion magnetic anisotropy energy (MAE). Note that the summation  $\sum_{\langle i,j \rangle}$  runs over each bond connecting the sites  $i$  and  $j$  only once. The  $4f$ -part is described explicitly with the total magnetic moment  $\mathbf{J} = \mathbf{L} + \mathbf{S}$  with  $\mathbf{L}$  being the orbital moment. The spin moment can be extracted via  $\mathbf{S} = (g_J - 1)\mathbf{J}$  with  $g_J$  being Landé's  $g$ -factor. Describing a  $4f$ -moment of Nd<sup>3+</sup> with a classical spin of length  $g_J \sqrt{J(J+1)}$  with  $J = 9/2$  is semi-quantitatively justified within the scope of setting the target temperature range in 200 [K]  $\lesssim T \lesssim$  500 [K], with the  $J$ -multiplets separated in the scale of 1000 [K]. The  $4f$ - $4f$  exchange coupling terms,  $J^{\text{RR}}$ , in the scale of  $O(1)$  [K] have been dropped because our target energy scale to be realistically described is motivated by the typical operating temperature range 200 [K]  $\lesssim T \lesssim$  500 [K] of permanent magnets. Magnetic energy scales coming from  $J^{\text{RR}}$ 's are at most  $\sim 0.1T$  and should be washed out.

The  $4f$ - $3d$  indirect exchange coupling as denoted by  $J_{mi}^{\text{RT}}$  in Eq. (4) comes from  $(5d)^m$ - $(3d)^n$  ( $m \lesssim 1$  and  $n > 5$ ) exchange which is antiferromagnetic and RE on-site  $4f$ - $5d$  direct exchange which is ferromagnetic. Overall  $J_{mi}^{\text{RT}}$  is an antiferromagnetic coupling between the spin component of  $4f$  and  $3d$ , which means  $4f$  total moment

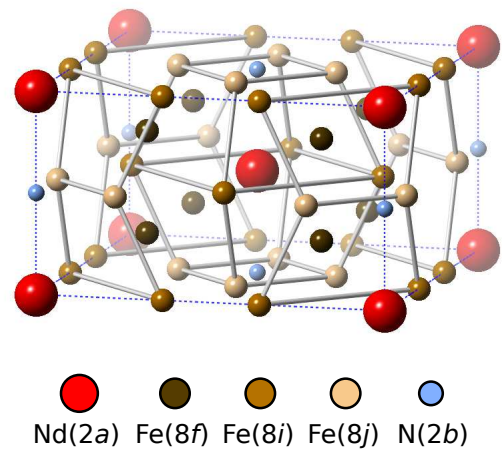


FIG. 1. Crystal structure of NdFe<sub>12</sub>N. Along the Nd(2a)-N(2b)-Nd(2a) direction runs the  $c$ -axis. Perpendicular to it, the other two equivalent directions,  $a$ -axis and  $b$ -axis, span the Nd(2a)-Fe(8i)-Fe(8i)-Nd(2a) lines.

and  $3d$  magnetization are ferromagnetically coupled for Nd<sup>3+</sup> with  $g_J = 8/11$ . The overall scale factor  $\alpha_{\text{RT}}$ , tentatively set to be one, has been introduced to phenomenologically describe the indirect nature of the  $4f$ - $3d$  exchange coupling.

### A. Derivation of the leading-order parameters

As shown in Fig. 1, the material NdFe<sub>12</sub>N has a ThMn<sub>12</sub> crystal structure (space group  $I4/mmm$ ) with Nd occupying the body-centered site of a tetragonal unit which incorporate 2 formula units. Around each Nd site, there are 4 Fe(8i) atoms which surround along the  $a$ -axis and  $b$ -axis. Four Fe(8j) atoms make a square right in the middle of Nd sites along the  $c$ -axis and nitrogen goes in the center of this square. Fe(8f) sites make a tetragonal box with the center occupied by Nd. Taking the ThMn<sub>12</sub> crystal structure as the starting point, the crystal structure is optimized from first principles. Then the crystal field parameters on Nd<sup>3+</sup> are calculated on the basis of open-core description for the  $4f$ -shell<sup>15</sup>. Up to here the calculations are done with the *ab initio* electronic-structure computational code package, QMAS<sup>16</sup>. The parameters for the exchange-coupling are calculated with the *ab initio* electronic-structure calculation code, Machikaneyama (AkaiKKR)<sup>17</sup>, using the Korringa-Kohn-Rostoker Green's function method, following the prescription proposed by Liechtenstein *et al.*<sup>18</sup>. Re-writing the term in Eq. (2) as  $J_{ij}^{\text{TT}} \mathbf{S}_i \cdot \mathbf{S}_j \equiv (S_i J_{ij}^{\text{TT}} S_j) \mathbf{e}_i \cdot \mathbf{e}_j$  with the vector  $\mathbf{e}_i$  denoting the direction of the magnetic moment on site  $i$ , calculated exchange couplings  $(S_i J_{ij}^{\text{TT}} S_j)$  are summarized in Fig. 2 (a) as a function of inter-site distance. As is the case for the champion magnet compound Nd<sub>2</sub>Fe<sub>14</sub>B<sup>19</sup>, we find that the dominant Fe-Fe exchange couplings come from Fe

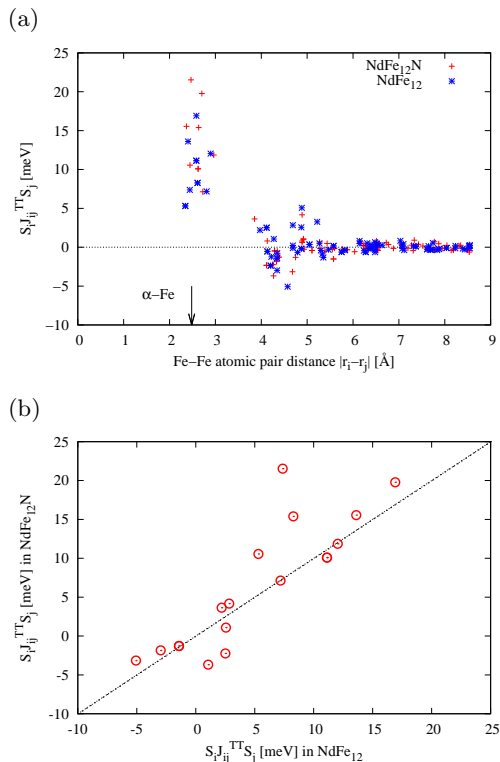


FIG. 2. (a) Calculated Fe-Fe exchange couplings as a function of Fe-Fe separation for  $\text{NdFe}_{12}$  and  $\text{NdFe}_{12}\text{N}$ . (b) The same data set is plotted on a plane spanned by  $J_{ij}(\text{NdFe}_{12})$  and  $J_{ij}(\text{NdFe}_{12}\text{N})$ , with  $J_{ij}$  shared among  $\text{NdFe}_{12}$  and  $\text{NdFe}_{12}\text{N}$  as the spatially equivalent bonds.

pairs whose interatomic distances almost coincide with that in  $\alpha\text{-Fe}$ . In our model we incorporate those dominant Fe-Fe exchange couplings, that can be classified into 8 classes on the realistic lattice for  $\text{NdFe}_{12}(\text{N})$  to make a leading-order description. Comparing the calculated exchange couplings on the same bonds located on the equivalent positions in the unit cell between  $\text{NdFe}_{12}$  and  $\text{NdFe}_{12}\text{N}$  as shown in Fig. 2 (b), nitrogenation-enhanced exchange couplings are identified. Interestingly, we observe those bonds are located along a kagomé-lattice network spanned by  $\text{Fe}(8f)$  and  $\text{Fe}(8j)$ , reminiscent of one-generation-back permanent-magnet materials family represented by  $\text{SmCo}_5$  with the strong magnetic anisotropy. The other leading-order term in the overall Hamiltonian written as Eq. (1) is  $4f$  single-ion MAE  $D_m^{\text{R}}(J_m^z)^2$ , which also shows up in the energy scale of  $O(10)$  [meV]. Rewriting the term in Eq. (3) as

$$D_m^{\text{R}}(J_m^z)^2 \equiv K_m^{\text{R}}(\mathbf{e}_m \cdot \mathbf{n})^2, \quad (5)$$

with  $\mathbf{n}$  denoting the direction of the easy axis and  $\mathbf{e}$  the direction of the total magnetic moment  $\mathbf{J}_m$  on the rare-earth site  $m$ , a QMAS calculation gives  $K^{\text{Nd}} = 5.8$  or  $11.0$  [meV] (easy-axis) for  $\text{NdFe}_{12}\text{N}$  and  $K^{\text{Nd}} = -3.0$  or  $-2.3$  [meV] (easy-plane) for  $\text{NdFe}_{12}$  depending on the

TABLE I. Calculated  $4f$ - $3d$  exchange couplings  $J_{mi}^{\text{RT}}$  in meV. The notation follows Eq. (4). The site index  $m$  denotes the Nd( $2a$ ) sublattice.

$i$	$\text{NdFe}_{12}$	$\text{NdFe}_{12}\text{N}$
$\text{Fe}(8i)$	1.58	1.90
$\text{Fe}(8j)$	1.54	1.00
$\text{Fe}(8f)$	1.93	2.36

calculation setups<sup>15</sup>. As a first step, we choose  $K^{\text{Nd}} = 8.1$  [meV] for  $\text{NdFe}_{12}\text{N}$  and  $= -2.8$  [meV] for  $\text{NdFe}_{12}$  within the range.

## B. Sub-leading parameters

We define  $J^{\text{RT}}$  and  $D^{\text{T}}$  in the overall Hamiltonian written as Eq. (1). Calculated antiferromagnetic exchange coupling between  $5d$ -bands of Nd and  $3d$ -bands of Fe are taken as they are to be the  $5d$ -mediated  $4f$ - $3d$  coupling, assuming that intra-atomic direct exchange coupling is big enough to let the localized  $4f$ -moment and  $5d$ -polarization work as a unified body. The results are summarized in Table I. The Fe-originated MAE in Eq. (2), which we will denote analogously to Nd-originated one in Eq. (5) as follows,

$$D_i^{\text{T}}(S_i^z)^2 \equiv K_i^{\text{T}}(\mathbf{e}_i \cdot \mathbf{n})^2 \quad (6)$$

comes in the order  $O(0.1)$  [meV] as referring to the past experimental measurements<sup>20</sup> done for  $\text{YFe}_{11}\text{Ti}$ . In the present modeling we just incorporate  $K^{\text{Fe}} = 0.1$  [meV] uniformly on all Fe sites as a phenomenological setting which should be sufficient to describe the magnetic properties around the room temperatures and slightly higher.

Higher-order terms in addition to  $K^{\text{Nd}}$  in Eq. (5) can be suspected in principle for which we have also calculated and saw that they are an order of magnitude smaller than the leading-order ones. Within the present scope to pick up the leading-order behavior of finite-temperature observables, we have dropped the higher-order contributions to the single-ion magnetic anisotropy of Nd.

## C. Methods

Having defined the realistic model basically from first principles for  $\text{NdFe}_{12}(\text{N})$ , the temperature dependence of the magnetic properties are calculated using the classical Monte Carlo method with the Metropolis local updates. We do one of the most plain local updates, that is, picking up lattice sites stochastically and proposing uniformly on the spherical spin space up to the stochastic decision referring to the energy difference as calculated by the spin model Hamiltonian defined as Eq. (1). Effective one lattice sweep, *i.e.* with the stochastic choice of the lattice

site to be updated done  $N_{\text{site}}$  times, is counted as one Monte Carlo step. Our input parameters are simply set to the  $T = 0$  *ab initio* values. For typical runs in the present work,  $10^5$  Monte Carlo steps (MCS) with each step consisting of a lattice sweep were sufficient to reach the thermal equilibrium state and subsequent  $10^6$  MCS are used for the numerical measurement of observables. The tetragonal unit of the body-centered-network of Nd is counted as a system-size unit in our calculation, thus a calculation with  $L \times L \times L$  system actually contains  $26L^3 \equiv N_{\text{site}}$  spins with the tetragonal unit having two formula units. Majority of the data are taken with  $L = 4$  which is sufficient as seen below with Fig. 4 (a) while the data points on the high-temperature side took system sizes up to  $L = 10$ , with the anisotropy field getting smaller and the calculated system getting closer to the Curie temperature where the finite system size can become an issue due to the diverging correlation length.

### III. RESULTS

With the prescription for the construction of the realistic-lattice spin model, calculated temperature dependence of magnetization and anisotropy field are shown in comparison with the experimental data<sup>5</sup>. Model parameter dependence of the overall calculated temperature dependence is inspected to draw our main conclusion:  $4f$ - $3d$  exchange couplings  $J_{mi}^{\text{RT}}$  in Eq. (4) dominates the observables in the operation temperature range *i.e.* around the room temperature or higher.

#### A. Magnetization

Calculated temperature dependence of magnetization  $M(T) \equiv \sqrt{M_x^2 + M_y^2 + M_z^2}$  for the bulk, the Nd-sublattice, and the Fe-sublattice of NdFe<sub>12</sub>N is shown in Fig. 3 (a). Calculated Curie temperature falls in the same range as the experimentally claimed one. Considering the possible presence of  $\alpha$ -Fe-originated noise in the experimental data and neglect of all next-nearest-neighbor exchange interactions in our model which should have lowered the computational magnetic-ordering energy scale, the agreement is satisfactory. Also we see that the system-size dependence is negligible in our focus temperature range, which up to  $T = 500$  [K] at most. Comparing the calculated temperature dependence of magnetization between NdFe<sub>12</sub> and NdFe<sub>12</sub>N as shown in Fig. 3 (b), we see that the experimentally observed<sup>5</sup> nitrogenation-triggered enhancement in the Curie temperature by  $\sim 200$  [K] is well reproduced.

We note that Nd in NdFe<sub>12</sub> has the easy-plane magnetic anisotropy<sup>5,15</sup> which would compete against the easy-axis anisotropy from at least a part of the Fe sublattices. Here we just track the origin of the difference in the Curie temperature between NdFe<sub>12</sub> and NdFe<sub>12</sub>N to the

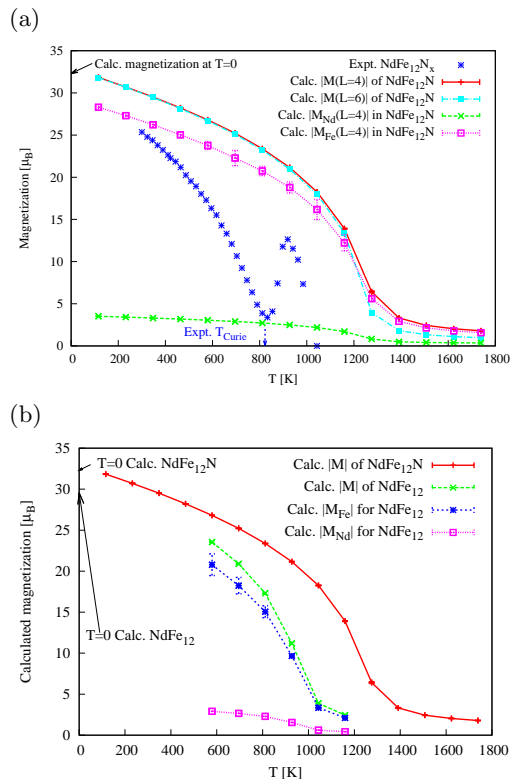


FIG. 3. (a) Calculated temperature dependence of magnetization for NdFe<sub>12</sub>N compared to the latest experimental data<sup>5</sup>. (b) Comparison of the calculated temperature dependence of magnetization between NdFe<sub>12</sub> and NdFe<sub>12</sub>N within  $L = 4$ .

nitrogenation-enhanced exchange couplings as demonstrated in Fig. 2. Further studies on the outcome of the competing anisotropies in NdFe<sub>12</sub> is separated for future work.

#### B. Anisotropy field

Calculated magnetization curves with the externally applied magnetic field parallel and perpendicular to the easy axis in NdFe<sub>12</sub>N (which is  $c$ -axis) at  $T = 348$  [K] is shown in Fig. 4 (a). The anisotropy field  $H_a$  is identified as a crossing point of the two curves with a linear fit. Our numerical measurement just follows the experimental way to determine  $H_a$ . Thus determined anisotropy field  $H_a(L, T)$  with the  $L$ -dependence being saturated out within the statistical error bars is plotted as a function of temperature in Fig. 4 (b) in comparison to the recent experimental data<sup>5</sup>. In the operation temperature range, a leading-order numerical control seems to be achieved.

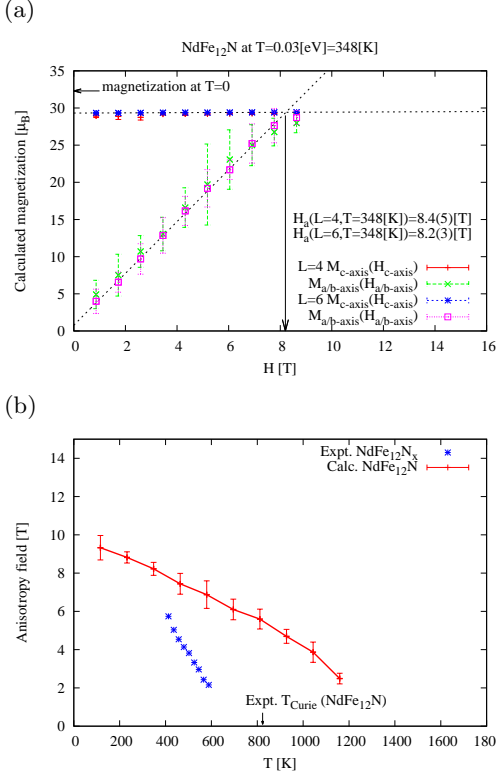


FIG. 4. (a) Numerical determination of the anisotropy field via the calculated magnetization curves for NdFe<sub>12</sub>N at  $T = 348$  [K] and (b) thus calculated temperature dependence of the anisotropy field for NdFe<sub>12</sub>N.

### C. Roles of each parameter

We inspect which parameter dominates which part of the temperature dependence of the observables comparing with the latest experimental data. One of the most important practical utilities of permanent magnets lies in the coercivity that is roughly proportional to the anisotropy field of the parent material or the main phase, and the main issue here is to figure out how to sustain the anisotropy field at high temperatures. Calculated MAE for Nd,  $K^{\text{Nd}}$ , and the input parameters for  $K^{\text{Fe}}$  obviously influence the temperature dependence of the anisotropy field. Flipping the sign of  $K^{\text{Fe}}$  for the Fe sublattice to have an easy-plane anisotropy, the overall reduction of the anisotropy field by  $2 \times 12 \times |K^{\text{Fe}}|/K^{\text{Nd}} \sim 30\%$  at the lowest temperature range is observed as shown in Fig. 5 (a). An interesting observation is made by enhancing  $K^{\text{Nd}}$  by 1/3 and flipping the sign of  $K^{\text{Fe}}$  at the same time, where the overall anisotropy field at the low-temperature side almost collapses onto the original temperature dependence as shown in Fig. 5 (b). The contribution of  $K^{\text{Fe}}$  is found to be quantitatively important in the bulk MAE at finite temperatures where an increase in the anisotropy field only by 10% can lead to a practical breakthrough in designing LRE-based magnets<sup>3</sup>. *Ab*

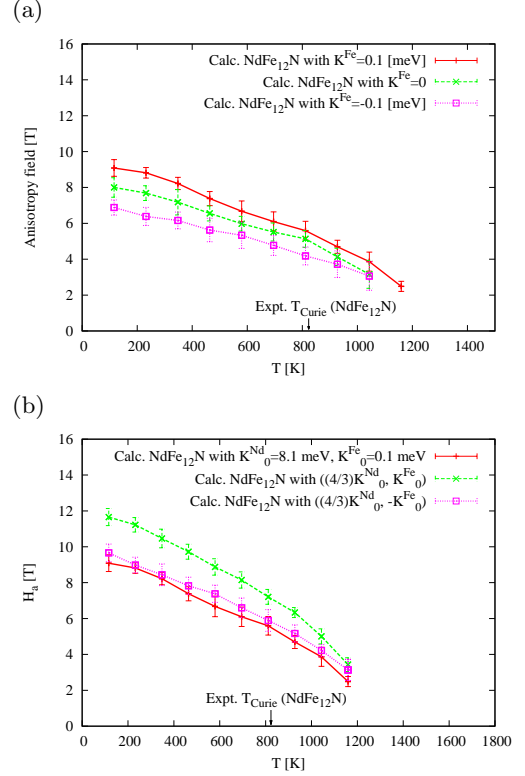


FIG. 5. ( $K^{\text{Nd}}, K^{\text{Fe}}$ )-trends of the calculated temperature dependence of the anisotropy field for NdFe<sub>12</sub>N. (a) Trends of  $H_a(T)$  with respect to  $K^{\text{Fe}} = \pm 0.1$  [meV]. Data with  $K^{\text{Fe}} = 0$  is also included as a reference. (b)  $K^{\text{Nd}}$  is enhanced by a fraction of 1/3 in observing the trends of  $H_a(T)$  with respect to  $K^{\text{Fe}} = \pm 0.1$  [meV].

*initio* determination of the exact nature of Fe-sublattice-dependent MAE is under way.

Numerically manipulating the *5d*-mediated *4f-3d* indirect exchange coupling,  $J^{\text{RT}}$ , we observe how the calculated temperature dependence of the magnetization and the anisotropy field in NdFe<sub>12</sub>N is affected as shown in Figs. 6 (a) and (b), respectively. The anisotropy field is more significantly affected by  $J^{\text{RT}}$  than the magnetization is especially around  $T \sim 300$  [K]. This is a numerical demonstration that a small enhancement in  $J^{\text{RT}}$ , which may be realized by the conduction-band engineering in *4f-3d* intermetallics, can already lead to a considerable improvement.

## IV. DISCUSSIONS

Having identified the quantitative relevance of  $J^{\text{RT}}_{mi}$  written as Eq. (4) for the magnetic properties of NdFe<sub>12</sub>N in the operation temperature range, we further pin-down the role of  $J^{\text{RT}}_{mi}$  in determining the realistic magnetic anisotropy energy scale at finite temperatures, through a close comparison between calculated results and the

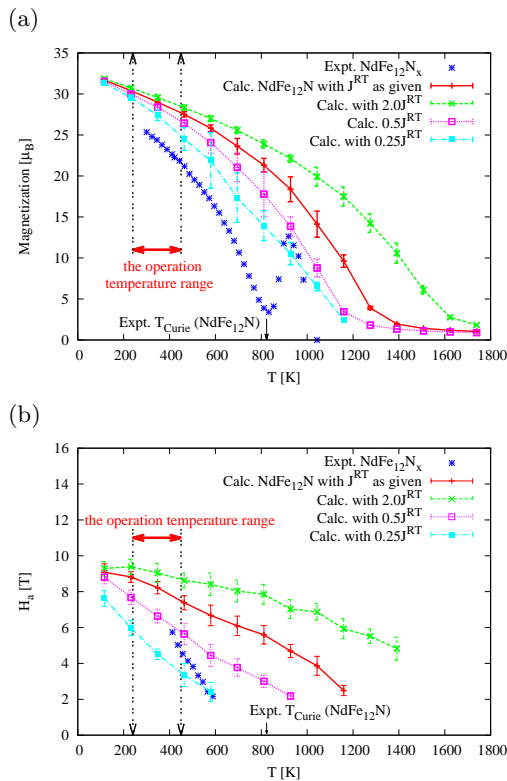


FIG. 6.  $J^{\text{RT}}$ -dependence of the calculated temperature dependence of (a) magnetization and (b) anisotropy field for  $\text{NdFe}_{12}\text{N}$ . Given values from the *ab initio* electronic-structure calculations are tabulated in Table I.

experimental data.

In Fig. 6, it is seen that the experimentally observed slope and the downward convexity of the temperature dependence of the anisotropy field for  $\text{NdFe}_{12}\text{N}$  is closest to the calculated  $H_a(T)$  with  $\alpha_{\text{RT}} = 0.25$ . Also the experimental anisotropy field near the liquid-nitrogen temperature seems to come close to 14 [T]<sup>21</sup> which suggests possible systematic underestimate in our calculated magnetic anisotropy which falls below 10 [T] in the limit  $T \rightarrow 0$ . The *ab initio* estimation for the crystal-field coefficients for the estimation of the uni-axial magnetic anisotropy energy indeed involves a certain uncertainty<sup>15</sup>.

An improved data collapse between theory and experiment in the lowest temperature range of  $H_a(T)$  can be observed by manually setting  $K^{\text{Nd}} = 2K_0^{\text{Nd}}$ . As shown in Fig. 7, the slope of the temperature dependence up to the room-temperature range is well reproduced. The upper shift of the calculated  $H_a(T)$  on the high-temperature side of the operation temperature range can be adjusted by a manual scaling of  $J^{\text{TT}}$  with an overall factor of 4/3 to match the Curie temperature. This can be considered as an effective renormalization of the  $3d$ - $3d$  exchange couplings imposed by the discarded longer-range part in the exchange couplings.

Thus an inspection of the experimental temperature

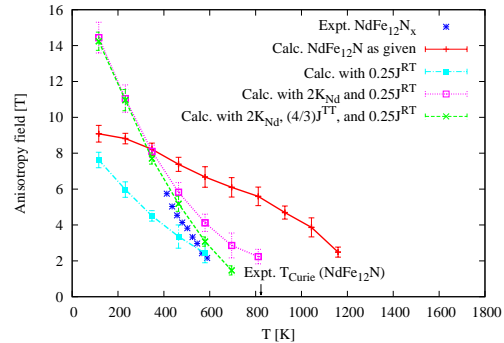


FIG. 7. For  $\text{NdFe}_{12}\text{N}$ , a data set which describes the experimental data most quantitatively comes with  $\alpha_{\text{RT}} = 0.25$ .

dependence of magnetization and anisotropy field leads to a set of model parameters for a quantitative description of the experimental finite-temperature data. Based on the obvious relevance of  $J^{\text{TT}}$  for the Curie temperature and  $K^{\text{R}}$  for  $H_a(T = 0)$ , it is seen that  $J^{\text{RT}}$  determines the slope of  $H_a(T)$  near  $T \gtrsim 0$ .

In such parameter set, the  $4f$ - $3d$  exchange couplings come close to a quarter of the tabulated numbers which were  $1 \sim 2$  [meV] as seen in Table I. In the language of the two-sublattice model<sup>10</sup> where an isolated  $4f$ -electron magnetic moment is put into the sea of  $3d$ -electron magnetization via a molecular field  $\mathbf{H}_m$ , the molecular field can be written in terms of our lattice model language as follows.

$$\mathcal{H}_m = \alpha_{\text{RT}} 2J^{\text{RT}} \mathbf{S} \times z_{\text{Nd}}$$

where  $z_{\text{Nd}}$  is the coordination number around the Nd magnetic moment which is in the present case  $z_{\text{Nd}} = 20$  within the nearest neighbor. Plugging in the realistic numbers  $\alpha_{\text{RT}} \sim 0.25$ ,  $J^{\text{RT}} \sim 2$  [meV],  $S \sim 2$  [ $\mu_B$ ] the magnitude of the exchange field is found to be  $H_m \sim 40$  [meV] = 700 [T] which gives the same order as was found in the experimental analyses  $H_m \sim 450$ –600 [T] by neutrons<sup>22</sup>.  $\alpha_{\text{RT}} = 1$  corresponds to  $H_m$  beyond 1000 [T] thus is out of the realistic scale. The smallness of the realistic number in the factor  $\alpha_{\text{RT}}$  presumably reflects the indirect nature of the  $4f$ - $3d$  exchange.

## V. CONCLUSIONS AND OUTLOOK

*Ab initio* modeling for the  $4f$  and  $3d$  magnetism coupled by  $5d$ -electrons on the basis of the realistic spin-lattice model for the rare-earth permanent magnet materials  $\text{NdFe}_{12}\text{N}$  and  $\text{NdFe}_{12}$  quantitatively captures the realistic energy scales in the leading order in the operating temperature range,  $200$  [K]  $\lesssim T \lesssim 500$  [K]. Experimentally observed magnetic ordering and magnetic anisotropy energy scales are put under numerical control and we have shown that enhancing the  $4f$ - $3d$  indirect

exchange coupling would work most effectively to realize the magnetic properties of more practical use in the operation temperature range. Establishing a quantitative description starting with the simplified model would pave the way to more realistic simulations to explicitly incorporate the strongly-correlated nature of  $4f$ -electrons embedded in the conduction-electron sea of  $5d$ -electrons to comprehensively describe the finite-temperature physics starting from the range  $T \gtrsim 1$  [K] all the way to the Curie temperature close to 1000 [K].

## ACKNOWLEDGMENTS

Helpful comments given by A. Sakuma, Y. Hirayama, and S. Hirosawa, and collaborative works in related projects with R. Banerjee and J. B. Staunton are gratefully acknowledged. This work is supported by the Elements Strategy Initiative Project under the auspice of MEXT, MEXT HPCI Strategic Programs for Innovative Research (SPIRE) and Computational Materials Science Initiative (CMSI).

- <sup>1</sup>M. Sagawa, S. Fujimura, N. Togawa, H. Yamamoto, and Y. Matsuura, *J. Appl. Phys.* **55**, 2083 (1984).
- <sup>2</sup>S. Hirosawa, Y. Matsuura, H. Yamamoto, S. Fujimura, M. Sagawa, *J. Appl. Phys.* **59**, 873 (1986).
- <sup>3</sup>K. Hono and H. Sepehri-Amin, *Scr. Mater.* **67**, 530 (2012).
- <sup>4</sup>T. Miyake, K. Terakura, Y. Harashima, H. Kino, and S. Ishibashi, *J. Phys. Soc. Jpn.* **83**, 043702 (2014).
- <sup>5</sup>Y. Hirayama, Y. K. Takahashi, S. Hirosawa, and K. Hono, *Scr. Mater.* **95**, 70 (2015).
- <sup>6</sup>Y. Hirayama, T. Miyake, and K. Hono, *JOM* **67**, 1344 (2015).
- <sup>7</sup>for a review, see e.g. J. Yang and Y. Yang, in *Handbook of Advanced Magnetic Materials*, Eds. Y. Liu, D. J. Sellmyer, and D. Shindo, Springer (2006).
- <sup>8</sup>M. Yamada, H. Kato, H. Yamamoto, and Y. Nakagawa, *Phys. Rev. B* **38**, 620 (1988).
- <sup>9</sup>J. M. Cadogan, J. P. Gavigan, D. Givord, and H. S. Li, *J. Phys. F: Met. Phys.* **18**, 779 (1988).
- <sup>10</sup>R. J. Radwański, *J. Mag. Mag. Mater.* **62**, 120 (1986); *Z. Phys. B* **65**, 65 (1986); R. J. Radwański and J. J. M. Franse, *Phys. Rev. B* **36**, 8616 (1987).
- <sup>11</sup>M. D. Kuz'min, *Phys. Rev. B* **46**, 8219 (1992); M. D. Kuz'min and J. M. D. Coey, *Phys. Rev. B* **50**, 12533 (1994).
- <sup>12</sup>M. Fähnle, K. Hummler, M. Liebs, and T. Beuerle, *Appl. Phys. A* **57**, 67 (1993).
- <sup>13</sup>R. Sasaki, D. Miura, and A. Sakuma, *Appl. Phys. Express* **8**, 043004 (2015).
- <sup>14</sup>R. Skomski, *J. Appl. Phys.* **83**, 6724 (1998).
- <sup>15</sup>Y. Harashima, K. Terakura, H. Kino, S. Ishibashi, and T. Miyake, *JPS Conf. Proc.* **5**, 011021 (2015).
- <sup>16</sup><http://qmas.jp>
- <sup>17</sup><http://kkcr.phys.sci.osaka-u.ac.jp>
- <sup>18</sup>A. I. Liechtenstein, M. I. Katsnelson, V. P. Antropov, and V. A. Gubanov, *J. Mag. Mag. Mater.* **67**, 65 (1987).
- <sup>19</sup>J. F. Herbst, *Rev. Mod. Phys.* **63**, 819 (1991).
- <sup>20</sup>S. A. Nikitin, I. S. Tereshina, V. N. Verbetskii, and A. A. Salamova, *Fiz. Tverd. Tela (St. Petersburg)* **40**, 285 (1998).
- <sup>21</sup>Y. Hirayama *et al.*, JIM meeting 2015, and private communications.
- <sup>22</sup>M. Loewenhaupt and I. Sosnowska, *J. Appl. Phys.* **70**, 5967 (1991).